Thermovibrational instability in supercritical fluids under weightlessness

S. Amiroudine[1,*] and D. Beysens[2,3]

[1]*LPMI-Arts et Métiers ParisTech, 2 Bd du Ronceray B.P., 93525, 49035 Angers, France*

[2]*ESEME, Ecole Supérieure de Physique et Chimie Industrielle, Laboratoire de Physique et Mécanique des Milieux Hétérogènes, 10, rue Vauquelin, 75231 Paris Cedex 05, France*

[3]*ESEME, Service des Basses Températures, CEA-Grenoble, Grenoble, France*

(Received 10 February 2008; revised manuscript received 16 July 2008; published 29 September 2008)

Low amplitude, high frequency vibrations can induce in fluids under weightlessness behaviors that resemble those induced by gravity. Supercritical fluids (above their gas-liquid critical point) are used in the space industry and also display universal behavior. They are particularly sensitive to gravity effects. When submitted to vibration (typically 0.1 to 0.5 mm amplitude, 10 to 50 Hz frequency), a Rayleigh-Bénard-like instability is observed in experiments with H_2 and CO_2 under weightlessness. The thermal boundary layer created during a temperature change displays periodic fingering perpendicular to the vibration direction. A systematic two-dimensional numerical study by the finite volume method is performed in CO_2 that shows that the fingering pattern is due to a thermovibrational instability, characterized by a vibrational Rayleigh number. The simulation and a simplified dimensional analysis show that the fingering wavelength and the vibrational Rayleigh number decrease as a power law with the distance in temperature to the critical point. However, due to the oversimplification of the analysis, the exponent in the simulation is found to be somewhat different than in the theoretical approach, calling for a more complete investigation of the problem.

DOI: 10.1103/PhysRevE.78.036325 PACS number(s): 44.25.+f, 47.20.Bp, 47.55.pb

I. INTRODUCTION

In space, in the absence of gravity effects, the behavior of fluids is markedly different than on Earth. The management of fluids in such conditions (flow control, heat exchange, etc.) is often a challenge and "artificial" gravity can be looked for. It happens that fluids submitted to vibrations of "high" frequency, e.g., frequency larger than the inverse hydrodynamics times (typically thermal diffusion and viscous dissipation times) and "low" amplitude (e.g., amplitudes smaller than the sample size) exhibit convective flows that are similar to buoyancy flows under earth gravity.

In this study, supercritical fluids (fluids above their critical point) are considered. The interest of studying fluids in such conditions is manifold. First, supercritical oxygen, hydrogen, and helium are already used in the space industry. Second, their high compressibility and slow dynamics ("critical slowing down") emphasize the behavior encountered in regular fluids. Third, fluids in such conditions obey universal, scaled power laws, valid for all fluids [1,2]. When these fluids are submitted to vibrations under weightlessness, it has been observed a number of intriguing phenomena, such as the layering of the gas-liquid phases [3], the acceleration of the gas-liquid phase transition dynamics [4,5], and Rayleigh-Bénard-like instabilities [6,7].

More specifically—and this is the object of the present study—a destabilization of thermal boundary layers was surprisingly observed in several weightless experiments when the fluid was vibrated [8,9]; periodic fingering was clearly visible, whose origin was puzzling. The thermal boundary layer (noted TBL in the following) is the region near the cell wall where the temperature gradient forms under a heating or cooling process. As outlined in the Appendix, the phenomena inside the TBL are indeed particularly important in the thermalization process of near-critical fluids.

In this paper, we present some fingering experiments and perform a set of numerical simulations that show that this instability is a Rayleigh vibrational instability as described in Ref. [10]. The instability originates in the TBL itself, as for the classical Rayleigh-Bénard instability in supercritical fluids [11].

II. EXPERIMENT

The observations were made when temperature was quenched down in experiments dedicated to study phase transitions under vibration. The fluid is submitted to a linear harmonic translational vibration in the x' direction, the latter perpendicular to the cylindrical axis (Figs. 1 and 2) as

$$x' = A' \cos\omega' t', \tag{1}$$

where A' is the vibration amplitude (typically 0.1–0.5 mm) and $\omega' = 2\pi f'$ is the angular frequency, with f' the frequency (typically 10–60 Hz). (All quantities with a prime stand for dimensional quantities).

The first set of experiments was concerned with a sample of hydrogen (H_2) at critical density. The cell is made with sapphire. The gravity effects are compensated by a magnetic field gradient [12]. The critical coordinates are $T'_c = 33.24$ K, $p'_c = 1.298$ MPa, and $\rho'_c = 30.09$ kg m^{-3}. This experiment was carried out in a cylindrical sample of 3 mm diameter and 3 mm thickness. Due to eddy currents, the temperature could not be directly measured and temperature stabilization could not be maintained for more than a few seconds. During the quench down from $\approx T'c+3$ mK to $\approx T'c+2$ mK, the TBL was always destabilized as shown in Fig. 1. Periodic fingers formed, with a mean distance λ'. Fuzzy fingers, out of the

*sakir.amiroudine@angers.ensam.fr

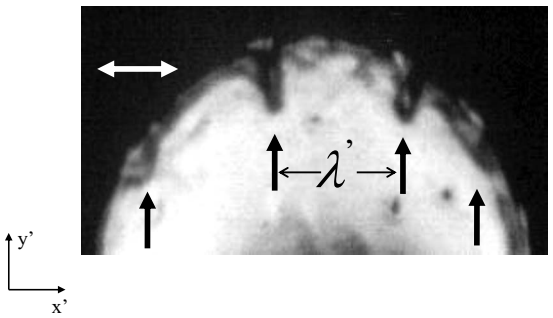

FIG. 1. Experimental observation of boundary layer fingering (arrows) in a cylindrical cell filled with H_2 under vibration (white arrow) $A'=0.4$ mm, $f'=50$ Hz when the boundary temperature is lowered from $\approx T_c'+3$ mK to $\approx T_c'+2$ mK. The mean distance between the fingers is $\lambda' \approx 0.8$ mm. Gravity was compensated by a strong magnetic field gradient as in Ref. [12]. Fuzzy fingers can also be detected, with the same λ' value.

focal plane, can also be detected, with the same λ' value. We cannot measure the distance between neat and fuzzy fingers, but it must be lower than the cell thickness.

The second set of experiments was carried out with a carbon dioxide (CO_2) sample filled at critical density in a sounding rocket (MAXUS 7, launched on May 2, 2006 in Esrange, Sweden). Details can be found in Refs. [3,9]. The critical data are in Table I. A thermostat containing the sample cell is vibrated by a shaker. The thermostat has temperature accuracy on the order of 0.5 mK. The shaker can apply linear harmonic vibrations in the range $A'=0.2-2.5$ mm and $f'=0.5-50.5$ Hz. The cell body is made with copper-beryllium. A cylindrical hole of 10 mm diameter, closed at each end by two parallel sapphire windows separated by 2.189 mm, contains the fluid. When quenching down to T_c', the same kind of fingering as in H_2 was observed (Fig. 2), with also fuzzy, out of focal plane fingers, which show the same λ' value. As for H_2, we cannot measure the distance between neat and fuzzy fingers, but it must be lower than the cell thickness.

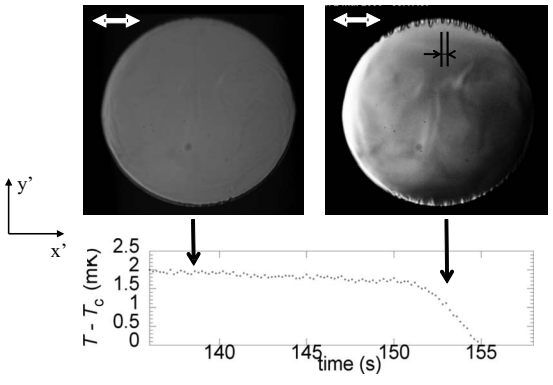

FIG. 2. Experimental observation of boundary layer fingering (arrows) in a cylindrical cell filled with CO_2 under vibration (white arrow) $A'=0.3$ mm, $f'=20$ Hz when the boundary temperature is lowered to T_c'. The mean distance between the fingers is $\lambda' \approx 0.3$ mm. Fuzzy fingers can also be detected, with the same λ' value. (MAXUS 7 sounding rocket, launched on May 2, 2006 in Esrange, Sweden).

TABLE I. Useful thermophysical data of CO_2 and Cu-Be.

	CO_2	Cu-Be
T_c' (K)	304.13	
ρ_c' (kg m^{-3})	468	8200
P_c' (MPa)	7.37	
β_P' (K^{-1})	$1.1\times10^{-3}\ \varepsilon^{-1.24}$	
χ_T (Pa^{-1})	$6.415\times10^{-9}\ \varepsilon^{-1.24}$	
$(\partial P' I \partial T')$ (Pa K^{-1})	1.70×10^{5}	
C_V' (J kg^{-1} K^{-1})	$1566\varepsilon^{-0.11}-1400$	
$C'p$ (J kg^{-1} K^{-1})	$120.53\varepsilon^{-1.24}$	419
c' (m s^{-1})	$160\varepsilon^{-0.055}$	
$\gamma_0 - C_p'/C_V'$	$7.69\times10^{-2}\ \varepsilon^{-1.13}$	
D_T' (m^2 s^{-1})	$5.997\times10^{-8}\ \varepsilon^{0.67}$	0.34×10^{-4}
ν' (m^2 s^{-1})	$9.0\times10^{-8}\varepsilon^{-0.04}$	
Λ' (W m^{-1} K^{-1})	$3.38\times10^{-3}\ \varepsilon^{-0.567}$	117
$\mathrm{Pr}=\nu'/D_T'$	$1.5\ \varepsilon^{-0.71}$	

III. MATHEMATICAL MODEL

We consider a square cavity (Fig. 3) of side length H' that contains supercritical CO_2 and is subjected to horizontal vibration in the x' direction, as shown in Fig. 3, with given amplitude A' and frequency f'. We assume weightlessness conditions. The fluid is initially maintained at a temperature T_0', then the temperature of the walls is lowered by an amount $\delta T' \ll T_0' - T_c'$. It was verified that quenching up gives results similar to quenching down, then all further studies will be only concerned with the boundaries submitted to a quenching down, as in the experiments. The density field is determined by the equation of state (see Sec. III A below). The pressure field is initially uniform.

A. Dimensionless equations

Our model is based on a Newtonian, compressible, viscous, supercritical fluid that conducts heat and is expandable in a nonstationary state. The dimensionless quantities are defined as follows: density $\rho=\frac{\rho'}{\rho_c'}$, pressure $p=\frac{p'}{\rho_c' c'^2}$, temperature

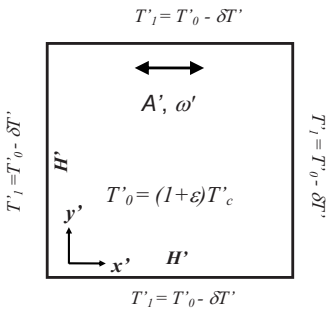

FIG. 3. Geometry of the numerical model. The cell is filled with supercritical CO_2 at critical density. Vibration (amplitude A', angular frequency ω') is imposed along the x' axis. The cell is initially at T_0', then the temperature is lowered by $\delta T'$ on each wall simultaneously.

$T=\frac{T'}{T'_c}$, space variables $\vec{x}=\frac{\vec{x}'}{H'}$, $\vec{y}=\frac{\vec{y}'}{H'}$, velocity $\vec{V}=\frac{\vec{V}'}{c'}$, and time $t=\frac{t'}{t'_a}$.

Here t' is time, $t'_a=\frac{H'}{c'}$ is the acoustic time scale, and c' is the sound velocity derived from the generalized Mayer equation

$$c' = \sqrt{\frac{p'_c}{\rho'_c}\left(\frac{p'_c\alpha_\rho^2}{\rho'_c C'_v T'_c}+\frac{1}{\chi_T}\right)}, \tag{2}$$

where $\alpha_\rho=\frac{T'_c}{p'_c}\left(\frac{\partial p'}{\partial T'}\right)_{\rho'}$, $\chi_T=\chi'_{T'}\rho'_c c'^2$ is the nondimensional isothermal compressibility and C'_v is the heat capacity at constant volume. The values of the above thermophysical properties correspond to the experimental data of CO_2 (Table I).

The dimensionless equations in weightless conditions can then be written as follows:

$$\frac{\partial \rho}{\partial t}+\nabla\cdot(\rho\vec{V})=0,$$

$$\rho\left[\frac{\partial \vec{V}}{\partial t}+(\vec{V}\cdot\vec{\nabla})\vec{V}\right]=-\vec{\nabla}p+\frac{1}{\mathrm{Re}}\left[\Delta\vec{V}+\frac{1}{3}\vec{\nabla}(\vec{\nabla}\cdot\vec{V})\right]+\frac{1}{\mathrm{Fr}_v^2}\rho\sin(\omega t)\vec{i},$$

$$\rho\left(\frac{\partial T}{\partial t}+\vec{V}\cdot\vec{\nabla}T\right)=\beta_P \mathrm{Ec}T\frac{dp}{dt}+\frac{1}{\mathrm{Re\,Pr}}\vec{\nabla}\cdot[\vec{\nabla}T]+\frac{\mathrm{Ec}}{\mathrm{Re}}\Phi,$$

$$\rho=\rho_0+\chi_T(p-p_0)-\beta_P(T-T_0). \tag{3}$$

Here Φ is the nondimensional dissipation rate defined as $\Phi=V_{i,j}V_{j,i}+V_{i,j}V_{i,j}-\frac{2}{3}V_{i,i}V_{j,j}$. The Einstein summation convention on repeated indices is applied. The dimensionless coefficients appearing in the above equations are $\mathrm{Fr}_v=\frac{c'}{\sqrt{H'(A'\omega^2)}}$ (vibration Froude number), $\mathrm{Pr}=\frac{\nu'}{D'_T}$ (Prandtl number), $\mathrm{Re}=\frac{H'c'}{\nu'}$ (Reynolds number), $\mathrm{Ec}=\frac{c'^2}{C'_p T'_c}$ (Eckert number), $\beta_P=\beta'_P T'_c$ (thermal expansion coefficient), $\omega=\omega' t'_a$ (dimensionless pulsation).

All the above dimensionless parameters are thus defined with respect to the supercritical physical properties and depend on only one control parameter $\varepsilon=\frac{T'-T'_c}{T'_c}$, which corresponds to the proximity to the critical point. The last equation in the system (3) corresponds to the equation of state. It is assumed to be linear [13,14] as the relative temperature difference $\delta T' \ll T'_0-T'_c$ [in the following $\delta T'=0.1(T'_0-T'_c)$]. The thermophysical properties χ_T and β_P can thus be assumed constant and evaluated at the initial state.

B. Numerical approach

Performing simulations near a critical point needs very long computational times. The reason comes from the fact that the properties vary considerably and the piston effect time scale reaches the acoustic time scale (acoustic saturation, see Ref. [15]). The compressibility becomes very large and solutions become numerically unstable. In order to remain within reasonable limits of costs, efforts, and time, we thus considered a two-dimensional simulation that we expect to capture the main features of the phenomenon. We thus assume implicitly—as is often the case (see, e.g., Ref. [10])—that the most instable mode in 2D is the same as in 3D. Note that the experiments were performed with a cell aspect ratio (thickness/diameter) of order 1 (H_2) and 0.2 (CO_2). It can then be reasonably claimed that at least the behavior in CO_2 can be described by a 2D simulation. Nevertheless, when looking carefully to the experiments in Figs. 1 and 2, fuzzy fingers are observed, which are not located in the focal plane. This is in agreement with the fact that the finger mean distance is smaller than the cell thickness. As the wavelength of neat and fuzzy fingers is the same, we can thus reasonably expect that 3D effects, although real, do not considerably affect the phenomenon in a section plane perpendicular to the cell axis.

TABLE II. Different characteristic times as a function of temperature: Piston effect time scale, t'_{PE}, thermal diffusion time t'_D, and the vibration periods. The viscous time scale is about $t'_\nu \approx 22$ min and the acoustic time scale is on the order of $t'_a \approx 0.6$ μs.

$T'-T'_c$	$t'_{\mathrm{PE}}\approx\frac{t'_D}{\gamma_0^2}$	$t'_D=\frac{H'^2}{D'_T}$	$t'^{10\ \mathrm{Hz}}_{\mathrm{vib}}$	$t'^{20\ \mathrm{Hz}}_{\mathrm{vib}}$	$t'^{80\ \mathrm{Hz}}_{\mathrm{vib}}$
30 K	11 min 8 s	2 h 11 min	0.1 s	0.05 s	0.0125 s
3 K	38.8 s	10 h 14 min			
2 K	22.5 s	13 h 25 min			
1 K	8.68 s	21 h 21 min			
0.3 K	1.58 s	47 h 50 min			
0.1 K	0.32 s	99 h 52 min			

The Navier-Stokes equations coupled with the energy and the equation of state and with the initial and boundary conditions are solved with a finite volume method by using the Simpler algorithm [15–17] in a staggered mesh. The space discretization uses the power-law scheme and time discretization is of first-order Euler. The time step is 10^{-3} s. In order to obtain the closed set of equations for average fields (as used in Ref. [10]), the vibration period has to be small with respect to all the characteristic time scales. In our case the period is 0.05 s, a time that is much smaller than the different characteristic time scales (see Table II), except the acoustic time scale which remains even smaller than the time step. The simulations are thus consistent with a time-averaged formulation as developed in Ref. [10]. The numerical code has been tested and used for many applications such as Boussinesq fluids, perfect gases, and highly compressible conditions (near-critical fluids) [14,15,17]. The grid size effect has been carefully tested. The viscous boundary layer thickness is of the order of $\delta_{\mathrm{vib}}=\sqrt{\frac{2\nu'}{\omega'}}\approx 46$ μm for $f'=20$ Hz. The kinematic viscosity is almost constant because the shear viscosity μ' exhibits a very low divergence $\mu'\sim\varepsilon^{-0.04}$. In all the studied cases, the nonuniform mesh has 80×80 points and the first point of the mesh is at about 14.3 μm. The integral form of the finite volume equations (which corresponds to the weak formulation) is, however, sufficient for filtering the above equations and getting numerical stability

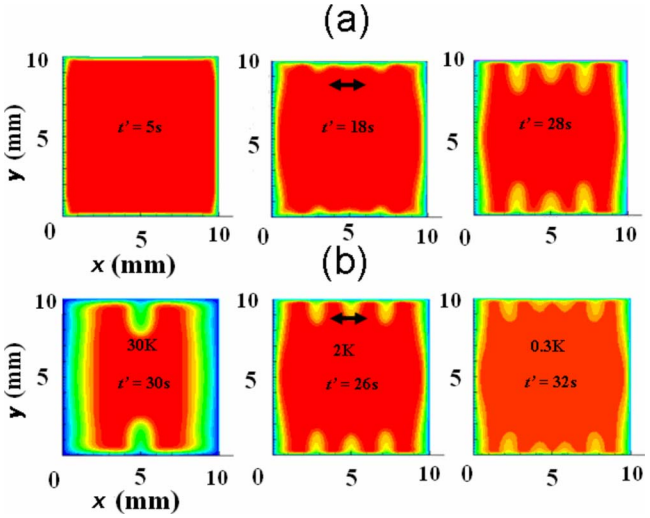

FIG. 4. (Color online) (a) Evolution of the numerical temperature field as a function of time for CO_2 in a square cell of 10 mm length when submitted to a temperature quench from T_c' +3 K to T_c'+2.7 K. (b) Temperature profiles at different initial temperatures $T'-T_c'=30$, 2, 0.3 K, with respective quenches of 3, 0.2, and 0.03 K and at different times 30, 26, and 32 s. Vibration (arrow): amplitude 0.5 mm, frequency 20 Hz.

even for time steps much larger than the acoustic time scale [14].

IV. RESULTS AND DISCUSSIONS

The experimental setup consisted of thin cylindrical cells. However, in the numerical simulation, we have considered a 2D square cavity (Fig. 3), with side $H'=10$ mm, submitted to a permanent vibration of 0.5 mm amplitude and 20 Hz frequency. This choice was dictated by the simpler situation and an easy comparison with already existing approaches [10]. It is anticipated that the results of the simulation will remain applicable, at least qualitatively, to the experimental cylindrical geometry. A detailed discussion of the comparison square–circle is given below in Sec. IV B. Some trials have been performed with rectangular cells with different aspect ratio 10 mm$\times$5 mm and 5 mm$\times$10 mm. The results were not significantly different. The temperatures investigated are $T_0'-T_c'=30$, 3, 2, 1, 0.3, and 0.1 K. The corresponding quenches are 3, 0.3, 0.2, 0.1, 0.03, and 0.01 K, keeping constant the ratio $\delta T'=(T'-T_c')/10$.

A. Observation

The numerical simulations give the same qualitative results as in the experiment. Figure 4(a) shows the time evolution of the temperature field. One can see the development of instabilities which occurs only in the horizontal boundaries, exactly as in the experiments (Figs. 1 and 2). Note that the wavelength does not change appreciably with time. In Fig. 4(b) are shown the patterns of the temperature field at different times and temperatures. The wavelength is seen to change with temperature with the closer the temperature to T_c, the smaller the wavelength.

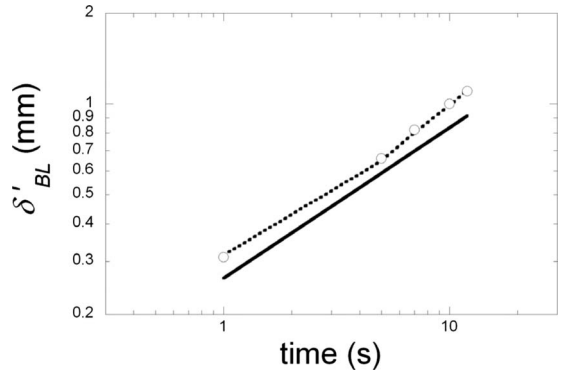

FIG. 5. Evolution of the thermal boundary layer thickness δ_{BL}' at $T'-T_c'=1$ K after a quench $\delta T'=0.1$ K (log-log plot). Vibration: $A'=0.5$ mm, $f'=20$ Hz. Circles and interrupted line: numerical data. Full line: $2\pi\sqrt{D_T't'}$.

We arbitrarily define the TBL thickness as the distance where the temperature reaches the uniform bulk temperature. The evolution of the thickness of the TBL before destabilization is shown in Fig. 5 during a quench of $\delta T'=0.1$ K from $T_0'-T_c'=1$ K. Keeping in mind the approximate definition of the layer thickness in the numerical experiment, the data compare very well with the classical diffusion growth law

$$\delta_{\mathrm{BL}}'=2\pi\sqrt{D_T't'}. \tag{4}$$

Here D_T' is the thermal diffusion coefficient, which goes to zero with ε as

$$D_T'\sim\varepsilon^{0.67}. \tag{5}$$

B. Analysis

The fingers that develop in the horizontal boundaries perpendicular to the vibration direction can be understood as a vibrational thermal instability [10], similar to a Rayleigh-Bénard instability [11,18,19]. Classically, the latter is concerned with a fluid layer confined between two horizontal isothermal walls separated by a length e' and submitted to gravity. The bottom wall is hotter than the top wall; the temperature difference is $\delta T'$. The Rayleigh-Bénard convection threshold is defined in terms of the Rayleigh number

$$\mathrm{Ra}=g'\frac{\beta_P'\delta T'e'^3}{\nu' D_T'}, \tag{6}$$

where g' is the earth acceleration of gravity. The fluid becomes unstable when $\mathrm{Ra}>\mathrm{Ra}_c\approx 1700$, where Ra_c is the critical Rayleigh number for the case of infinite solid-solid walls. A physical meaning of the Rayleigh number can be found by following a simple reasoning. Under earth gravity, a fluid element of size r_0' starts to rise when the typical convective time across the fluid element is shorter than the diffusion time to the surface, that is $\frac{r_0'}{V_{sg}'}<\frac{r_0'^2}{D_T'}$. Here V_{sg}' is the Stokes convective velocity as given by

$$V'_{sg} = \frac{2r_0'^2 \Delta\rho' g'}{9\rho'_c \nu'} = \frac{2r_0'^2 g' \beta'_P \delta T'}{9\nu'}. \quad (7)$$

The equation $\Delta\rho' = \rho'_c \beta'_P \delta T$ has been used. The Rayleigh number gives then a measure of the ratio of both diffusive and convective times.

When the temperature T' approaches the critical temperature T'_c, Ra diverges and the fluid becomes extremely unstable. However, owing to the thermal characteristics of the Piston effect (see Appendix A), the temperature gradient forms only in the thermal boundary layer [11]. A simple means to account for this new situation is to replace e' by δ'_{BL}, whose evolution is temperature dependent through D'_T [see Eq. (4) and Table I]:

$$\delta'_{\mathrm{BL}} \propto (T' - T'_c)^{0.335}. \quad (8)$$

A saturation of the instability takes place because the fluid becomes compressed under its own weight. Another instability occurs, corresponding to the gradient that is obtained by adiabatically rising up a fluid particle along the hydrostatic pressure gradient, leading to the so-called Schwarzschild criterion. This notion is commonly used in atmospheric science [20]. In weightlessness, neither the Rayleigh-Bénard nor the Schwarzschild criteria are applicable anymore, but the fluid remains sensitive to vibrations. Vibrations induce different velocities to density inhomogeneities by inertial effects. Mean flows can be provoked and, as in the thermal configuration of the Rayleigh-Bénard case, a vibrational Rayleigh number can be constructed as [10]

$$\mathrm{Ra}_\nu = \frac{(A'\omega'\beta'_P \delta T' e')^2}{2\nu' D'_T}. \quad (9)$$

The physical meaning of this vibrational Rayleigh number can be found by following the same reasoning that leads to the definition of the classical Rayleigh number. The criterion for buoyancy-driven convection can be replaced by the presence of a Bernoulli-like pressure difference coming from the velocity difference $\Delta V'$ between the fluid element and its surrounding, $\Delta p' \approx \rho'_c \Delta V'^2 = \rho'(\Delta\rho'/\rho'_c)^2 A'^2 \omega'^2_2$. It results in a driving force $r_0'^2 \Delta p'$, oriented perpendicularly to the vibration direction. Applying the same procedure used to define the Rayleigh number, another number is obtained, the vibrational Rayleigh number [see Eq. (9)].

Convection starts for Ra_ν above a critical number Ra_{ν_c}. According to the reasoning developed above where the Bernoulli pressure drives the convection perpendicular to the vibration direction, the onset of instability will crucially depend on the angle α' between the vibration and the temperature gradient direction. When $\alpha' = 0$, the pressure difference drives any inhomogeneities along the temperature isotherms. The fluid is thus stable, $\mathrm{Ra}_{\nu_c} = \infty$ (for small α', the asymptotic form is $\mathrm{Ra}_v \sim \alpha^{-4}$ [10]). When α' increases to $\pi/2$, Ra_{ν_c} decreases to a value of the order of 2100, which is comparable to the classical critical Rayleigh number in the Rayleigh-Bénard configuration. Note that the variation of Ra_v becomes steep for $\alpha' < \alpha'_0 \approx 50° - 60°$ [10]. This angle determines indeed the limits of the fingering pattern in Figs. 1 and 2 (Fig. 1: $\alpha'_0 \approx 40°$; Fig. 2: $\alpha'_0 \approx 53°$). In other words, the equivalent square cell of a circular cell of radius R' would have a side length $H' \approx R'$.

The critical value $\mathrm{Ra}_{\nu_c} = 2100$ corresponds to the case of a vibrated layer in contact on both sides with infinite walls of much larger thermal conductivity than the fluid. The above condition is always met on the solid wall (Table I): the Cu-Be wall conductivity (117 W m^{-1} K^{-1}) is always larger than the CO_2 conductivity, although diverging. (At a temperature as small as $T' - T'_c = 1$ μK, $\Lambda'_{\mathrm{CO}_2} = 8.6$ W m^{-1} K^{-1}.) However, it is clear that Ra_{ν_c} should differ from 2100 in the present situation where only one finite solid wall is present. This point was already noticed in Ref. [10] in nonstationary states when the Prandtl number $\mathrm{Pr} = \nu'/D'_T$ takes large values. This situation is precisely met here (see Table I) and means that the instability indeed develops in the TBL during the transient. In addition, the fluid conductivity in the boundary layer and in the bulk varies much when going to T_c (it diverges, see Table I), then the Ra_{ν_c} value should also vary with $T - T_c$.

Because of mass conservation, convection rolls eventually form (such rolls have been observed in the simulations on 2D incompressible and inviscid fluids [10]). From the temperature dependence of β'_P, υ', and D'_T (Table I), one gets

$$\mathrm{Ra}_v \sim (T' - T'_c)^{-3.11} (\delta T' e')^2 \sim (T' - T'_c)^{-1.11} e'^2. \quad (10)$$

From Eq. (9) and the expression δ'_{BL} [Eq. (4)], it comes that

$$\mathrm{Ra}_v = \frac{(A'\omega'\beta'_P \delta T' \delta'_{\mathrm{BL}})^2}{2\nu' D'_T} = \frac{2\pi^2 (A'\omega'\beta'_P \delta T')^2 t'}{\nu'}, \quad (11)$$

which shows that, at constant temperature, Ra_v increases proportionally with time. At given (constant) time, Ra_v increases when going near T'_c as

$$\mathrm{Ra}_v \sim \varepsilon^{-0.44}. \quad (12)$$

The time $t' = t'_c$ where the instability starts can be determined from the simulations. When reported in Eq. (11), it thus gives the critical Rayleigh number Ra_{ν_c}. The corresponding values are reported in Fig. 6. It is clear that Ra_{ν_c} increases strongly when approaching T'_c, as

$$\mathrm{Ra}_{\nu_c} = R_{1,2} \varepsilon^{-m}. \quad (13)$$

Two limiting behaviors can be fitted to the two following power laws: near T'_c, $R_1 = (0.95 \pm 0.70) \times 10^3$ with $m_1 = 0.86 \pm 0.1$ and far from T'_c, $R_2 = (26 \pm 8) \times 10^3$ with $m_2 = 0.31 \pm 0.06$ (the uncertainties correspond to one standard deviation). The temperature variation of Ra_{ν_c} is not surprising, as discussed above. It can be attributed to the changes of thermal conditions throughout the thermal boundary layer and the bulk fluid. The exact determination of its temperature dependence needs a full linear stability analysis and is out of the scope of the present study.

Figure 7 displays a typical evolution of the temperature field as a function of x' near the bottom wall. After an initial state (about 20 s that corresponds to a transient regime), the wavelength keeps almost constant, which permits one to determine it without ambiguity. The wavelength can then be evaluated under these two conditions: (i) after the initial tran-

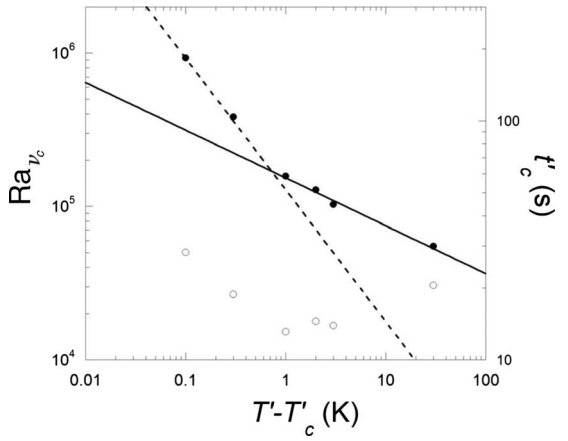

FIG. 6. Left ordinate: critical vibrational Rayleigh number (full dots) with respect to relative temperature as deduced from the critical time t'_c (right ordinate, open dots) in Eq. (11). The lines are fit to the power law Eq. (13) of the data near (interrupted line) and far (full line) from T'_c (vibration $A'=0.5$ mm, $f'=20$ Hz).

sient regime and (ii) in the middle of the x' axis, in order to get rid of the boundary effects.

In Fig. 8 is reported the evolution of the wavelength λ' as a function of temperature for various numerical simulations. λ' decreases with temperature, as already observed in Fig. 4(b) and can be fitted to the two power laws

$$\lambda' = \lambda'_{1,2}\varepsilon^{n_{1,2}}. \tag{14}$$

Near T'_c, $\lambda'_1=(2.32\pm05)$ mm with $n_1=0.06\pm0.03$ and far from T'_c, $\lambda'_2=(4.5\pm0.08)$ mm with $n_2=0.172\pm0.005$ (the uncertainties correspond to one standard deviation). If one assumes that, as for the Rayleigh-Bénard instability, $\lambda'\sim\lambda'_c$ at the threshold, one gets from Eq. (11):

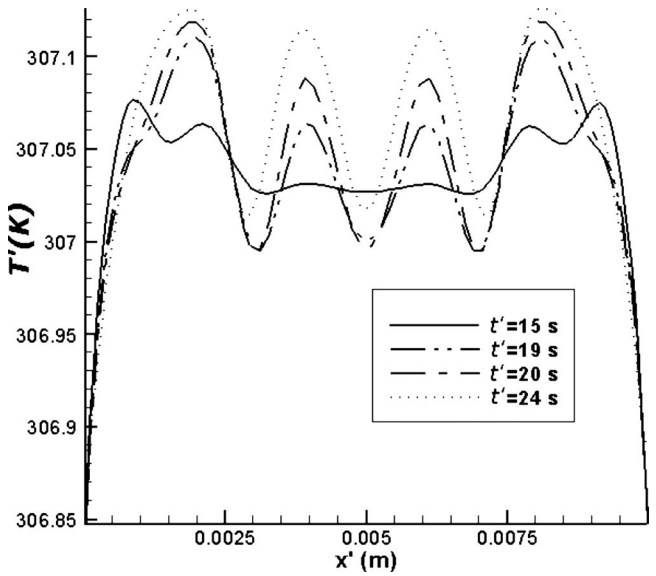

FIG. 7. Evolution of the temperature field as a function of the x' coordinate at the bottom of the cavity ($y'=0.23$ mm) and at different times. Vibration: $A'=0.5$ mm, $f'=20$ Hz; temperature $T'-T'_c=3$ K.

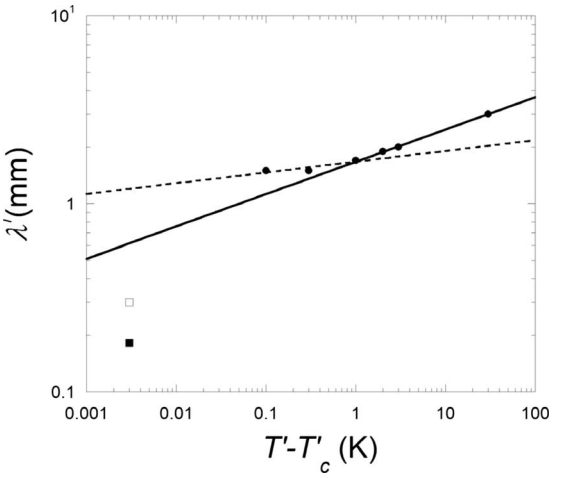

FIG. 8. Variation of the wavelength λ' with respect to $T'-T'_c$ (semilog plot). Full circles: numerical values (vibration: $A'=0.5$ mm, $f'=20$ Hz). Empty square: experimental data (vibration: $A'=0.3$ mm, $f'=20.2$ Hz). Full square: experimental data extrapolated according to Eq. (15) to $A'=0.5$ mm and $f'=20$ Hz. The lines are fit to the power law Eq. (14) of the data near (interrupted line) and far (full line) from T'_c (vibration $A'=0.5$ mm, $f'=20$ Hz).

$$\lambda' \approx \delta'_c \approx \frac{\sqrt{2\nu' D'_T \mathrm{Ra}_{v_c}}}{A'\omega'\beta'_P\Delta T'} \sim \varepsilon^{n_i} \tag{15}$$

that should go to zero with the exponent $n_i=\frac{1.11-m_i}{2}$. Taking into account the two exponent values $m_i=m_1$ or m_2 it comes, near T'_c, $n_1=0.12$ and far from T'_c, $n_2=0.4$. The exponent value is, alike the experimental exponent, larger far from T'_c than close to T'_c. The values, however, differ by about a factor 2, a result that reflects the limits of this simulation (2D) and the assumptions made concerning the similarity of a two-conductive walls Rayleigh-Bénard arrangement with the thermal boundary layer configuration.

V. CONCLUDING REMARKS

A general issue to manage fluids in space might be the use of high frequency, low amplitude vibrations that act as an artificial gravity. In this exploratory study we were more particularly concerned with thermovibrational convections. Experiments carried out in a weightless environment have shown surprising periodic fingering at the boundary of a vibrated supercritical fluid submitted to a temperature quench. The present numerical simulation, although only 2D, exhibits similar behavior, which can be explained in terms of a Rayleigh thermovibrational instability. The associated critical vibrational Rayleigh number is seen to diverge near the critical point while the instability wavelength goes to zero when nearing T_c. Further work is planned to better describe and understand this instability.

ACKNOWLEDGMENTS

The authors gratefully acknowledge the financial support from CNES Space Agency, CNRS and the IDRIS Computing Center (Orsay). They also thank the ESA Space Agency for

providing us with the MAXUS 7 sounding rocket flight. They thank Y. Garrabos, P. Evesque, and D. Chatain for their support in the experiments, J. Ouazzani for help in the numerical simulations and V. Nikolayev for a critical reading of the manuscript.

APPENDIX

When heating or cooling the wall of a cell containing a fluid, a thermal boundary layer (TBL) forms, of thickness δ':

$$\delta \sim \sqrt{D'_T t'}. \tag{A1}$$

In near-critical fluids, this thickness develops very slowly since D'_T goes to zero at T'_c. The thermal expansion coefficient diverges, strongly expanding the TBL (or contracting when cooling). Large density gradients form in the TBL although the temperature gradients stay very small. This expansion (or contraction) is at the origin of a very efficient mechanism of temperature equilibration, the "piston effect" [21–25], where the TBL expands and pressurizes the whole sample. It results in a fast and uniform temperature rise in the bulk. In contrast to the well-known "critical slowing down" due to the vanishing thermal diffusivity, this process results instead in a "critical speeding up" of thermalization.

When a temperature quench is applied to the wall of the cell, the temperature in the bulk, T'_b, relaxes from its initial temperature T'_0 towards the final temperature of the wall T'_f as [24,25]

$$T'_b - T'_f \sim \left(\frac{t'}{t'_{\mathrm{PE}}}\right)^{-1/2}, \tag{A2}$$

with T'_{PE} is the piston effect typical time

$$t'_{\mathrm{PE}} = \frac{L'^2}{D'_T(\gamma_0 - 1)^2} \approx \frac{L'^2}{D'_T \gamma_0^2}. \tag{A3}$$

Here, L' is a typical cell length scale and γ_0 is the ratio of the specific heats at constant pressure and volume that diverges near the critical point as $\gamma_0 \sim \varepsilon^{-1.13}$. Then T'_{PE} tends to zero when T' tends to T'_c as $t'_{\mathrm{PE}} \sim \varepsilon^{1.59}$.

[1] H. E. Stanley, *Introduction to Phase Transitions and Critical Point Phenomena* (Oxford University Press, Oxford, 1971).
[2] A. Onuki, *Phase Transition Dynamics* (Cambridge University Press, Cambridge, 2002), and references therein.
[3] R. Wunenberger, P. Evesque, C. Chabot, Y. Garrabos, S. Fauve, and D. Beysens, Phys. Rev. E **59**, 5440 (1999).
[4] D. Beysens, D. Chatain, P. Evesque, and Y. Garrabos, Phys. Rev. Lett. **95**, 034502 (2005).
[5] D. Beysens, Europhys. News **37**, 22 (2006).
[6] Y. Garrabos, D. Beysens, C. Lecoutre, A. Dejoan, V. Polezhaev, and V. Emelianov, Phys. Rev. E **75**, 056317 (2007).
[7] D. Beysens, D. Chatain, Y. Garrabos, P. Evesque, C. Lecoutre, F. Palencia, and V. Nikolayev, Acta Astron. **61**, 1002 (2007).
[8] D. Beysens (unpublished).
[9] D. Beysens, Y. Garrabos, D. Chatain, and P. Evesque, Europhys. Lett. (to be published).
[10] G. Z. Gershuni and D. V. Lyubimov, *Thermal Vibrational Convection* (Wiley, New York, 1998).
[11] S. Amiroudine, P. Bontoux, P. Larroudé, B. Gilly, and B. Zappoli, J. Fluid Mech. **442**, 119 (2001).
[12] R. Wunenburger, D. Chatain, Y. Garrabos, and D. Beysens, Phys. Rev. E **62**, 469 (2000).
[13] S. Amiroudine, K. Boutrouft, and B. Zappoli, Phys. Fluids **17**, 054102 (2005).
[14] K. Boutrouft, S. Amiroudine, and A. Ambari, Phys. Fluids **18**, 124106 (2006).
[15] S. Amiroudine, J. Ouazzani, B. Zappoli, and P. Carles, Eur. J. Mech. B/Fluids **16**, 665 (1997).
[16] S. Patankar, *Numerical Heat Ttransfer and Fluid Flows* (McGraw Hill, New York, 1980).
[17] S. Amiroudine and B. Zappoli, Phys. Rev. Lett. **90**, 105303 (2003).
[18] A. B. Kogan and H. Meyer, Phys. Rev. E **63**, 056310 (2002).
[19] Y. Chiwata and A. Onuki, Phys. Rev. Lett. **87**, 144301 (2001).
[20] M. Gitterman, Rev. Mod. Phys. **50**, 85 (1978).
[21] A. Onuki, H. Hao, and R. A. Ferrel, Phys. Rev. A **41**, 2256 (1990).
[22] H. Boukari, J. N. Shaumeyer, M. E. Briggs, and R. W. Gammon, Phys. Rev. A **41**, 2260 (1990).
[23] B. Zappoli, D. Bailly, Y. Garrabos, B. Le Neindre, P. Guenoun, and D. Beysens, Phys. Rev. A **41**, 2264 (1990).
[24] A. Onuki, H. Hao, and R. A. Ferrell, Phys. Rev. A **41**, 2256 (1990).
[25] Y. Garrabos, M. Bonetti, D. Beysens, F. Perrot, T. Fröhlich, P. Carlès, and B. Zappoli, Phys. Rev. E **57**, 5665 (1998).